AFRL-PR-WP-TP-2006-247

MIXING EFFECTS OF PYLON-AIDED FUEL INJECTION LOCATED UPSTREAM OF A FLAMEHOLDING CAVITY IN SUPERSONIC FLOW (POSTPRINT)

Lt. Daniel R. Montes, Paul I. King, Mark R. Gruber, Campbell D. Carter, and Kuang–Yu (Mark) Hsu

JULY 2005

Approved for public release; distribution is unlimited.

STINFO COPY

PROPULSION DIRECTORATE
AIR FORCE MATERIEL COMMAND
AIR FORCE RESEARCH LABORATORY
WRIGHT-PATTERSON AIR FORCE BASE, OH 45433-7251

REPORT DOCUMENTATION PAGE

Form Approved
OMB No. 0704-0188

1. REPORT DATE *(DD-MM-YY)*	2. REPORT TYPE	3. DATES COVERED *(From - To)*
July 2005	Conference Paper Postprint	09/01/2004 – 07/31/2005

4. TITLE AND SUBTITLE

MIXING EFFECTS OF PYLON-AIDED FUEL INJECTION LOCATED UPSTREAM OF A FLAMEHOLDING CAVITY IN SUPERSONIC FLOW (POSTPRINT)

5a. CONTRACT NUMBER
In-house

5b. GRANT NUMBER

5c. PROGRAM ELEMENT NUMBER
62203F

6. AUTHOR(S)

Lt. Daniel R. Montes and Paul I. King (Air Force Institute of Technology)
Mark R. Gruber and Campbell D. Carter (AFRL/PRAS)
Kuang–Yu Hsu (Innovative Scientific Solutions, Inc.)

5d. PROJECT NUMBER
3012

5e. TASK NUMBER
AI

5f. WORK UNIT NUMBER
00

7. PERFORMING ORGANIZATION NAME(S) AND ADDRESS(ES)

Air Force Institute of Technology
WPAFB, OH 45433

Propulsion Sciences Branch (AFRL/PRAS)
Aerospace Propulsion Division
Propulsion Directorate
Air Force Research Laboratory
Air Force Materiel Command
Wright-Patterson AFB, OH 45433-7251

Innovative Scientific Solutions, Inc.
Dayton, OH 45440

8. PERFORMING ORGANIZATION REPORT NUMBER
AFRL-PR-WP-TP-2006-247

9. SPONSORING/MONITORING AGENCY NAME(S) AND ADDRESS(ES)

Propulsion Directorate
Air Force Research Laboratory
Air Force Materiel Command
Wright-Patterson AFB, OH 45433-7251

10. SPONSORING/MONITORING AGENCY ACRONYM(S)
AFRL-PR-WP

11. SPONSORING/MONITORING AGENCY REPORT NUMBER(S)
AFRL-PR-WP-TP-2006-247

12. DISTRIBUTION/AVAILABILITY STATEMENT
Approved for public release; distribution is unlimited.

13. SUPPLEMENTARY NOTES
Conference paper published in the Proceedings of the 41st AIAA/ASME/SAE/ASEE Joint Propulsion Conference and Exhibit, published by AIAA.

 PAO case number: AFIT/PA 060860; Date cleared: 05 September 2006. Paper contains color.

14. ABSTRACT

An investigation into the non-reacting flow associated with the pylon-aided gaseous fuel injection upstream of a flame holding cavity is described. Characteristics of penetration and mixing were measured in a Mach 2 freestream environment. The downstream combustion cavity had an LID of 4.7 and an aft ramp angle of 22.5 degrees. A circular injection port was placed upstream of the cavity, and a series of three pylons (medium, tall, wide geometries) were in turn fitted just upstream of the port to examine changes in mixing and penetration of the fuel into the core airflow. The main goals of this experiment were to characterize the mixing ability of injected fuel with the core flow as it propagated downstream of the pylon and to analyze the effects, if any, of this mixing strategy on cavity flow and overall efficiency compared to a no pylon case. Visual measurements were obtained using Planar Laser-Induced Fluorescence (PLIF), and Mie scattering techniques. Of the three pylon geometries tested, the wide pylon (1.6 jet diameters wide, 4 diameters high) provided a 135% increase in penetration.

15. SUBJECT TERMS
Supersonic combustion, fuel injection, laser-based diagnostics

16. SECURITY CLASSIFICATION OF:			17. LIMITATION OF ABSTRACT:	18. NUMBER OF PAGES	19a. NAME OF RESPONSIBLE PERSON (Monitor)
a. REPORT	b. ABSTRACT	c. THIS PAGE			Mark R. Gruber
Unclassified	Unclassified	Unclassified	SAR	28	19b. TELEPHONE NUMBER *(Include Area Code)* N/A

Standard Form 298 (Rev. 8-98)
Prescribed by ANSI Std. Z39-18

41st AIAA/ASME/SAE/ASEE Joint Propulsion Conference & Exhibit
10 - 13 July 2005, Tucson, Arizona

AIAA 2005-3913

Mixing Effects of Pylon-Aided Fuel Injection Located Upstream of a Flameholding Cavity in Supersonic Flow

Lt. Daniel R. Montes[*] and Paul I. King,[†]
Air Force Institute of Technology, Wright-Patterson AFB, OH, 45433

Mark R. Gruber[‡] and Campbell D. Carter,[§]
Air Force Research Laboratory (AFRL/PRAS), Wright-Patterson AFB, OH, 45433

and

Kuang-Yu (Mark) Hsu[**]
Innovative Scientific Solutions, Inc., Dayton, OH, 45440

An investigation into the non-reacting flow associated with the pylon-aided gaseous fuel injection upstream of a flame holding cavity is described. Characteristics of penetration and mixing were measured in a Mach 2 freestream environment. The downstream combustion cavity had an L/D of 4.7 and an aft ramp angle of 22.5 degrees. A circular injection port was placed upstream of the cavity, and a series of three pylons (medium, tall, wide geometries) were in turn fitted just upstream of the port to examine changes in mixing and penetration of the fuel into the core airflow. The main goals of this experiment were to characterize the mixing ability of injected fuel with the core flow as it propagated downstream of the pylon and to analyze the effects, if any, of this mixing strategy on cavity flow and overall efficiency compared to a no pylon case. Visual measurements were obtained using Planar Laser-Induced Fluorescence (PLIF), and Mie scattering techniques. Of the three pylon geometries tested, the wide pylon (1.6 jet diameters wide, 4 diameters high) provided a 135% increase in penetration. The tall pylon (1.1 jet diameters wide, 6 diameters high) improved penetration by 190% but incurred a large loss penalty. Lower injection pressures experienced a greater improvement in penetration height (pylon versus flat) and lower shock losses than injection at higher pressures. All pylons lifted the fuel from the injection wall in the farfield (a flashback related issue), and all pylons demonstrated distinctive mixing characteristics when compared to the flat reference, although quantifying experiments on this subject are recommended.

Nomenclature

q	=	dynamic pressure ratio	h	=	pylon height
P_0	=	total pressure	θ	=	pylon wedge angle
L	=	cavity length	y_j	=	fuel jet penetration height
D	=	cavity depth	Δy	=	fuel jet vertical spread
X_f	=	distance from injector to cavity	Δz	=	fuel jet horizontal spread
X_p	=	proximity of pylon to injector	g	=	floor gap
ℓ	=	pylon length	A_j	=	fuel jet cross-sectional area
W	=	pylon width	A_s	=	fuel jet standard deviation area

[*] Currently with AFRL/MN, Eglin AFB, FL, Nonmember.
[†] Professor, Department of Aeronautics and Astronautics, AFIT/ENY, AIAA Senior Member
[‡] Senior Aerospace Engineer, AIAA Associate Fellow
[§] Senior Aerospace Engineer, AIAA Associate Fellow
[**] Senior Research Scientist, AIAA Senior Member

I. Introduction

A key area of study to advance supersonic combustor development is the characterization of cavity-based fuel injection and flameholding. Cavity-based flameholders are commonly found in hydrocarbon-fueled scramjet combustors, but low residence time and interactions with disturbances in the main air flow (i.e., shock trains or shock-boundary layer interactions) raise issues on which detailed information is largely unavailable in the existing literature.[1]

One area of interest concerns the creation of disturbances in the main flow by the use of small pylon devices. Provided that aerodynamic drag and shock losses are minimized, injection behind a pylon has many advantages. Combined with injection, the shock-jet interactions created by these devices cause vorticity via baroclinic torque and cross-stream shear and may improve mixing.[1] This concept may be applied to an upstream pre-injection mechanism that aims to provide a well mixed flow over a downstream cavity. Injection behind pylons also causes an increase in the penetration height of the fuel for a given dynamic pressure ratio, defined later.

The penetration effect serves to conceivably enhance mixing, shorten the isolator and combustor (the two components of a dual mode scramjet combustion system), and possibly simplify the fuel control system. The effect also lifts fuel out of the boundary layer, a technique that prevents flashback (ignition of fuel that has been seeded into the subsonic boundary layer) as has been shown in the case of liquid injection.[2]

In this investigation, a pylon was aligned upstream of a normal, sonic, circular injector so that the fuel jet could be studied as it propagates downstream. Three pylon sizes with several injection pressures as well as a no pylon baseline were employed in this experiment. The hardware was installed with injection immediately behind the pylon and at a distance of 0.9L (cavity lengths) upstream of the cavity employed by Gruber et al.[3] Each pylon is a thin triangular wedge with a 30^o inclination angle. Optimal pylon heights, widths, and pylon distances from injection were determined from previous computational research[4] and correlate with sizes used in prior experimentation.[1-2] The investigation included measuring the effects of penetration height and width, shock effects, mixing effectiveness and pressure profiles. The purpose of this research was to determine 1) The effect of pylons on basic jet geometries, such as penetration height, plume width (as seen from profile and end views), floor separation, and cross-sectional area, as compared to the no pylon case, and the preventability of flashback, 2) Affected mixing potential, in the form of visible structures and measured standard deviation intensity and turbulent mixing area, 3) The effect of pylons on the supersonic airflow (through a visual examination of bow shocks).

II. Procedures and Methodology

A. Hardware

Experiments were conducted in a Mach 1.98, P_0 = 50 psia flow environment supplied by a supersonic combustion research facility located at AFRL/PR. More details on the tunnel capabilities may be found in the facility paper.[5] For information on current and past cavity studies using this facility, refer to Gruber et al.[3] Optical access of the test section is available through three fused silica windows: one on each side wall and another on the top wall. The nozzle exit is 2 inches high by 6 inches wide, located where viewing becomes available through the side wall windows. The test section is comprised of a constant area isolator (7-inches long) and a 2.5-degree divergent combustor (30-inches long). The fused silica windows provide excellent optical opportunities and transmissive properties for visualization equipment. Each side window provides access to the entire transverse dimension, while the top window allows viewing of half the spanwise dimension (window is 3 inches wide).

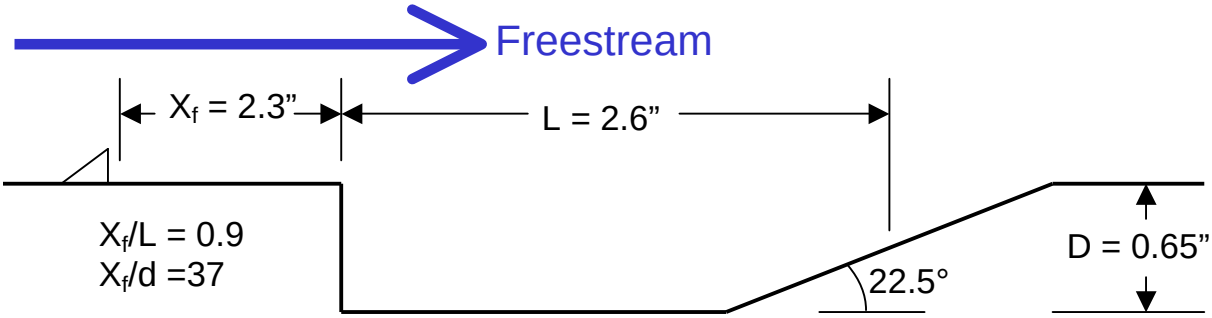

Figure 1. AFRL designed cavity with pylon installed upstream

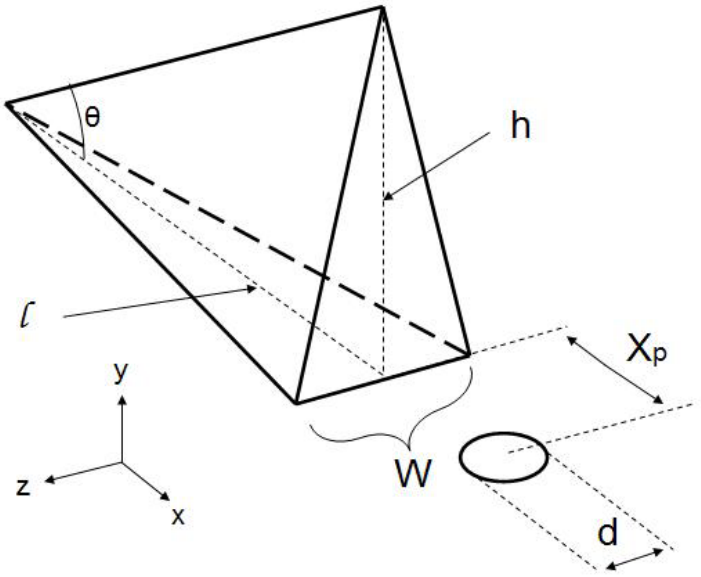

Figure 2. Pylon geometry shown with injection port and defined axis system

The cavity assembly (including upstream pylons) was installed along the first 12 inches of the bottom wall on the diverging ramp using a configurable base plate. The cavity has a length (L) of 2.6 inches, and a depth (D) of 0.65 inches. The cavity is recessed in the floor with a 90 degree rearward facing step, and the trailing edge contains a 22.5 degree ramp. L/D = 4. The upstream injector is located at a distance (X_f) of 2.3 inches in front of the cavity leading step. The injection diameter (d) is 1/16 inch. Figure 1 shows the measurement convention (not to scale).

Separate studies by Livingston and Segal and by Owens et al. established pylon geometries that were used for liquid injection experimentation.[1-2] Gouskov et. al performed a numerical analysis of gaseous jet injection behind pylons, and the results from various geometries and injection distances were tabulated.[4] All three of these studies estimated penetration height to equal about 1.5 times the pylon height. Based on the top two configurations found to enhance fuel penetration height and using a wedge angle established by the liquid injection studies, three pylons were designed for this experiment. Figure 2 shows a diagram of the pylon, injection port, and their geometric properties. The streamwise (x), transverse (y), and spanwise (z) axes are labeled. The origin of this coordinate system lies on the center of the injection port at the surface.

Table 1. Pylon dimensions for Medium, Tall, and Wide geometries

d = 0.0625 in	Medium (M)	Tall (T)	Wide (W)
Height: h (in)	0.25	0.375	0.25
Length: ℓ (in)	0.43	0.65	0.43
Width: W (in)	0.07	0.07	0.1
Proximity: X_p (in)	0.14	0.14	0.2
Wedge Angle: θ (deg)	30.2	30	30.2
h/d	4	6	4
W/d	1.12	1.12	1.6
Xp/d	2.24	2.24	3.2

Injection diameter (d) is 1/16 inch for all the cases that were tested. X_p is the injection proximity to the pylon, measured from the pylon base to the centerline of injection. The three independent geometric parameters on the pylon were chosen as length, width, and height (ℓ, W, and h, respectively). The wedge angle (θ) is derived from ℓ and h. The two parameters that were emphasized in the numerical study were X_p and W. Two pylons in this experiment were designed using the optimal case ($X_p/d \approx 2$, $W/d \approx 1$). One is termed the Medium (M) pylon and is 1/8 the height of the test section (0.25"). The larger pylon is termed Tall (T) and is 3/16 the height of the test section (0.375"); it is designed to differ from Pylon M only in length and height but preserve width and angle. The third pylon uses the second best case ($X_p/d \approx 3$, $W/d \approx 1.5$), and is termed the Wide (W) pylon. It has the same length and height as Pylon M and has a larger X_p and W. In all three pylons, $X_p/W \approx 2$ and $\theta \approx 30°$ as previous liquid fueling studies used the same approximate wedge angle in their geometries. Pylon dimensions are presented in Table 1.

The pylon may be removed to provide a baseline case, termed the Flat (F) condition. Simulated fuel was injected in the transverse direction at three values of dynamic pressure ratio (q). These values are 3.0, 1.5, and 0.75 (termed Injections 1, 2, and 3 respectively). This yields twelve pylon/injection combinations. Injection at q = 0.75 using the Medium pylon will be referred to as the M3 case, for example.

B. Visualization

Instantaneous measurements of the fuel jet at various locations were obtained by both Mie scattering and Planar Laser-Induced Fluorescence of nitric oxide (NO-PLIF). For Mie scattering, the simulated fuel was dry, compressed air. Visualization was obtained by a laser sheet scattering from ice crystals present in the freestream flow, contrasted against the dry fuel jet which does not emit a scattering signal. Shocks, boundary layer, and other viscous or thermal effects are detectable when the freestream ice crystals melt and do not produce scattering signals. This produces images that qualitatively characterized the jet fluid, associated shocks, and boundary layer heating. In the NO-PLIF measurements, the injected air was seeded with a 1% NO in N_2 mixture. This mixture was adjusted to produce about 1,000 ppm of NO in the total jet mixture. NO-PLIF relies on fluorescence to produce images that capture the presence of NO in the fuel jet (and thus capture the fuel jet). Although this method is qualitative in

nature, the species-specific images capture mixing developments that conventional visual methods and Mie scattering cannot reveal.[6]

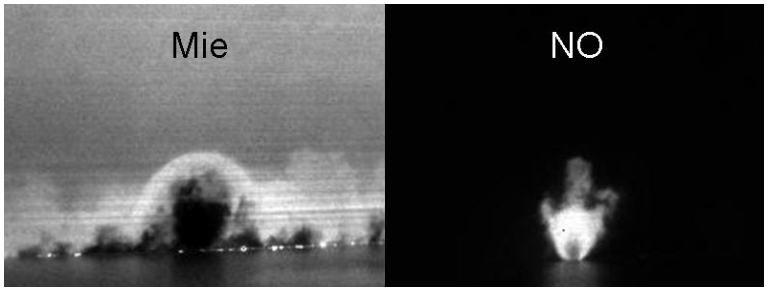

Figure 3. Comparison of visualization methods

In order to access the NO A-X state transitions, the laser system consisted of a Lumonics Hyperdye dye laser and an injection-seeded Spectra Physics® Nd: YAG laser (GCR-170). The second harmonic of the Nd: YAG was pumped into the dye laser. The dye output was frequency doubled and then frequency mixed with residual IR output from the Nd: YAG using Inrad® Autotraker III's to produce frequency mixed radiation at 226 nm. A sample signal was monitored on an oscilloscope to ensure good overlap of the laser and transition. Using this, small adjustments were made to the dye laser grating position to account for temperature variance on the signal. The concentration of NO in the fuel mixture was kept nearly constant to retain a relatively constant electronic quenching rate and mole fraction of NO and produce a clear fluorescence signal for every hardware/injection configuration. The images themselves were not corrected for discrepancies in electronic quenching, collisional line broadening, laser coupling effects, or ground state population. Although signal strength varies slightly with the above phenomena (which depend on core pressure and temperature), a decrease in signal intensity can be taken to represent a decrease in NO concentration and therefore mixing and dilution of the jet fluid with the freestream.

The laser sheet was created using a plano-concave cylindrical lens (negative 50 mm focal length) and a plano-convex spherical lens (1000 mm focal length). The resulting sheet height was roughly 75 mm, and thickness is estimated at 250 – 300 μm. Scattering and fluorescence were both captured normal to the laser sheet using a Princeton Instruments® PIMAX intensified CCD Camera. The camera was fitted with a 45 mm focal length f/1.8 Cerco® UV lens. For NO-PLIF measurements, a UG-5 filter was used to block scattering at 226 nm and collect fluorescence from the (0,1), (0,2), and (0,3) bands. This filter was not required for Mie scattering measurement. For streamwise view (profile) images, the laser sheet was directed down through the top wall window and centered on the injection centerline; imaging occurred normal to the sheet through a side wall window. For spanwise (end) views, the sheet was transmitted over the test section span through the side wall windows, and imaging took place from a side window as well. Eight locations were chosen, with 0 corresponding to fuel jet center as defined previously in the pylon section. Marching the laser sheet downstream (x direction), the distances are 0 (jet center), 0.25, 0.5, 0.75, 1.0, 1.25, 1.5, and 2.0 inches downstream of injection (x/d = 0, 4, 8, 12, 16, 20, 24, 32). Because the camera was positioned at an off-normal angle to the sheet, the image was corrected for blur by employing a Scheimpflug mount.

End views were captured for all twelve cases. Profiles were acquired for the Medium and Flat cases (six total). Each capture consisted of 200 instantaneous images. Instantaneous images capture large scale turbulent structures that form at the interaction between the jet and the core flow, as well as development and unsteadiness of the bow shock and jet penetration through the boundary layer (Mie scattering only). A set may be sum averaged into mean images to trace fluid spread, or a standard deviation may be obtained to qualitatively observe turbulence and mixing potential. Figure 3 demonstrates instantaneous data for both visualization methods. The presence of jet fluid, boundary layer, and shocks is seen as the dark regions of the instantaneous and mean Mie examples, whereas the jet fluid is the white region in the NO images. For NO-PLIF, higher standard deviation intensities are represented as whiter regions. Before performing measurements on the images, they were corrected for camera skew using linear interpolation, and the test section floor was removed.

III. Results

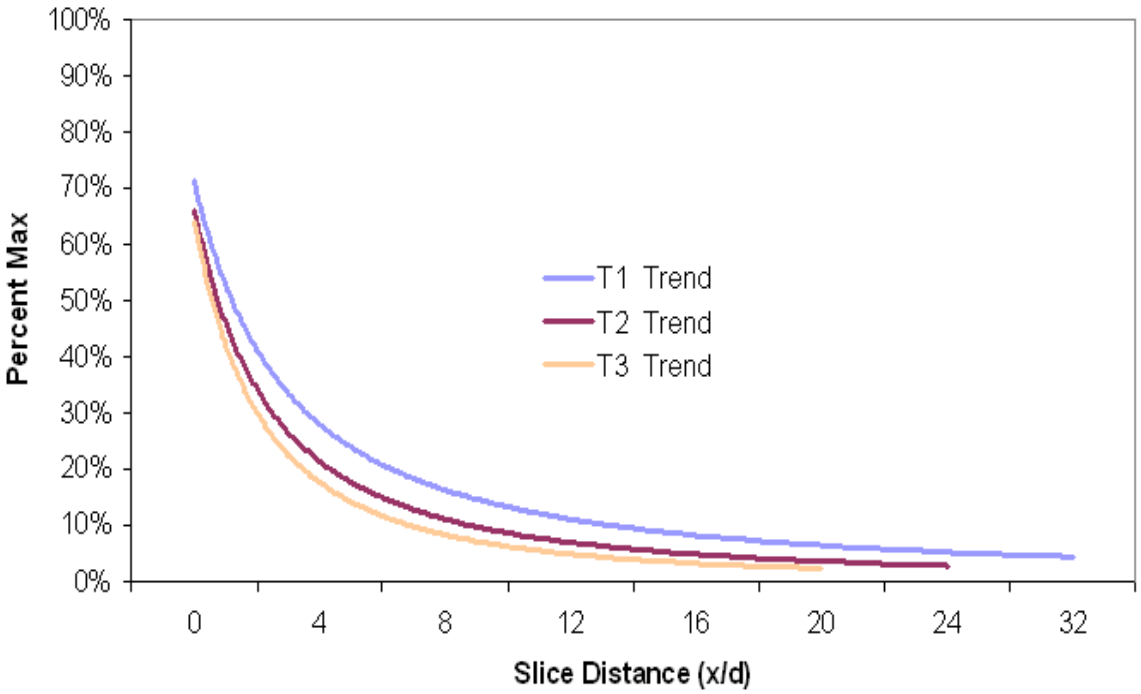

Figure 4. Decrease in maximum value of jet concentration with several injection pressures

A. Image Intensities

In addition to cropping and skew-correcting images, laser sheet and hardware inconsistencies were subtracted during post-processing in order to produce the most accurate data possible. It was necessary to adjust the brightness scale on resulting images in order to bring out features in the data that are not normally visible in the raw pictures. This does not present a problem with Mie scattering data, as the stark contrast between dark and light regions is clear, and the presence of fuel jet, shocks, and boundary layer are visible and qualitatively measurable. Likewise, standard deviation images (Mie and NO-PLIF) present areas of interaction within a given frame of observation, so adjusting brightness to accentuate the local maximum is desirable.

Of interest is the decrease in the value of the local maximum in the mean NO images as the end view camera traverses downstream of injection (positive x direction). The mean NO information is directly related to jet fluid concentration, thus trend lines for the maximum readings have been plotted in the x direction normalized by the value of the max reading at x = 0 (directly over injection). Figure 4 shows these trends for the Tall pylon. The other pylons and the flat injection exhibited similar behavior, in that the q = 0.75 case (injection pressure 3) resulted in the jet diluting fastest into the freestream.

A similar analysis was performed on the NO standard deviation data. As expected, the standard deviation intensity, as compared to the maximum at injection, did gradually decrease in the same manner as observed in Figure 4. There were inconsistencies though, attributed to the fact that standard deviation is a product of many factors, including fuel/air interaction and localized turbulence. The pylons retained more standard deviation intensity than the no pylon case, which suggests more global interaction. This can be related to mixing. When brightness is rescaled, local interactions are visually detectable. In the same way, rescaling the brightness in the mean NO images was performed as a next step in order to perform calculations on jet geometry. These processes are discussed in the following section.

B. End Views

Figure 5 below shows sample instantaneous captures. The raw images may be referenced in order to grasp the nature of the complicated flow, especially at the interface between jet fluid and freestream flow. Those structures suggest a large mixing interface (seen with all cases) which is not evident from the averaged images. These interfaces exist in the layer between the jet fluid and the incident shockwave, which previous research confirms.[7] Large formations are a good indicator of mixing potential. Further conclusions are drawn from standard deviation results. Figures 6 through 9 show the mean and standard deviation images at q = 3 for all four hardware types at locations of 0, 1, and 2 inches downstream of injection.

Both Mie scattering and NO-PLIF images were visually rescaled so that the bulk of usable data was presented across a full (0 – 255) grayscale. Mie scattering images were rescaled to provide suitable detection of bow shocks and jet fluid. NO images were specifically scaled so that the maximum local value of each image was assigned to 255 (white) and the zero value to 0 (black). This allows for suitable measurements of local phenomena in both mean and standard deviation images.

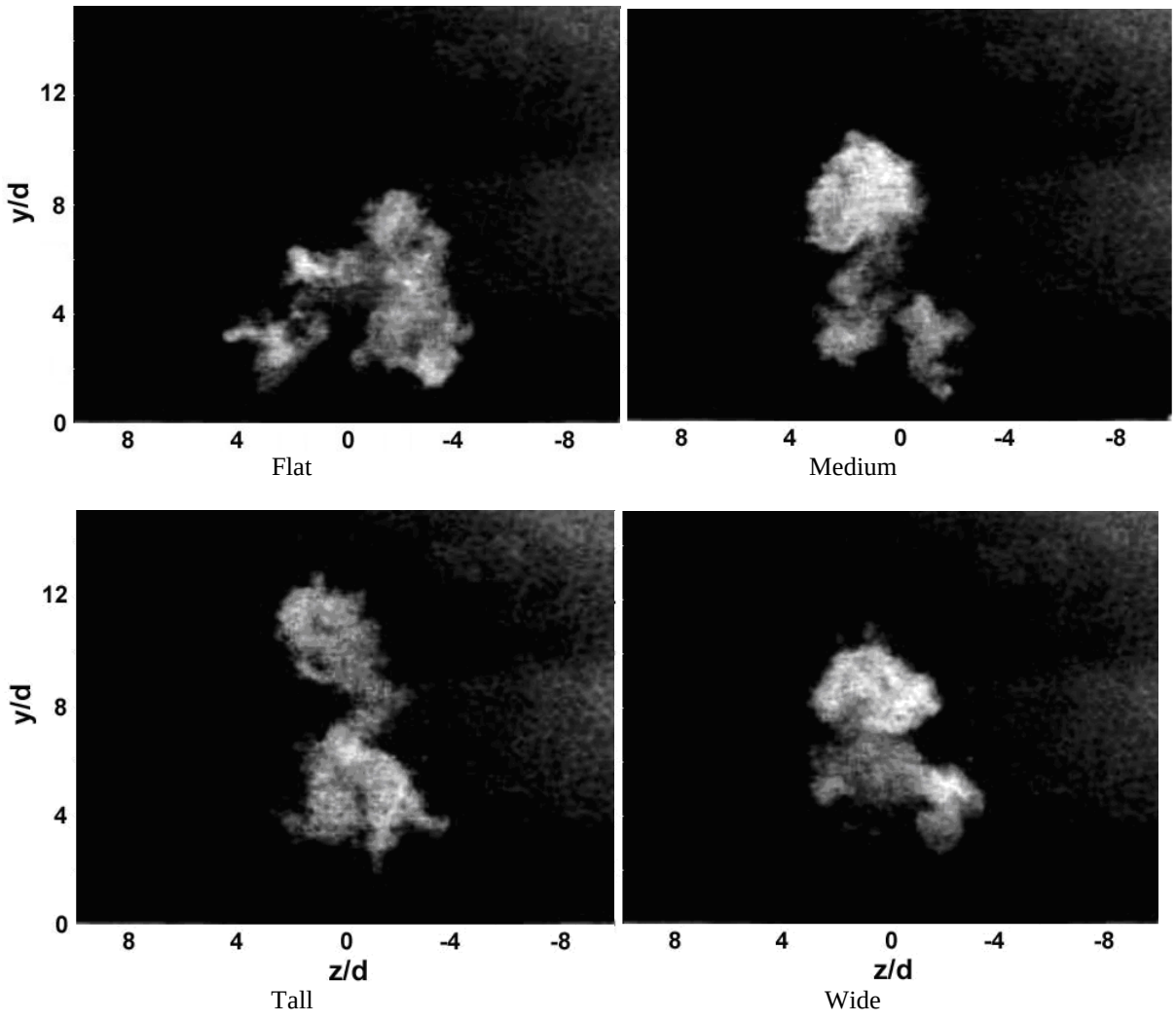

Figure 5. Instantaneous NO-PLIF end view images (x/d = 16)

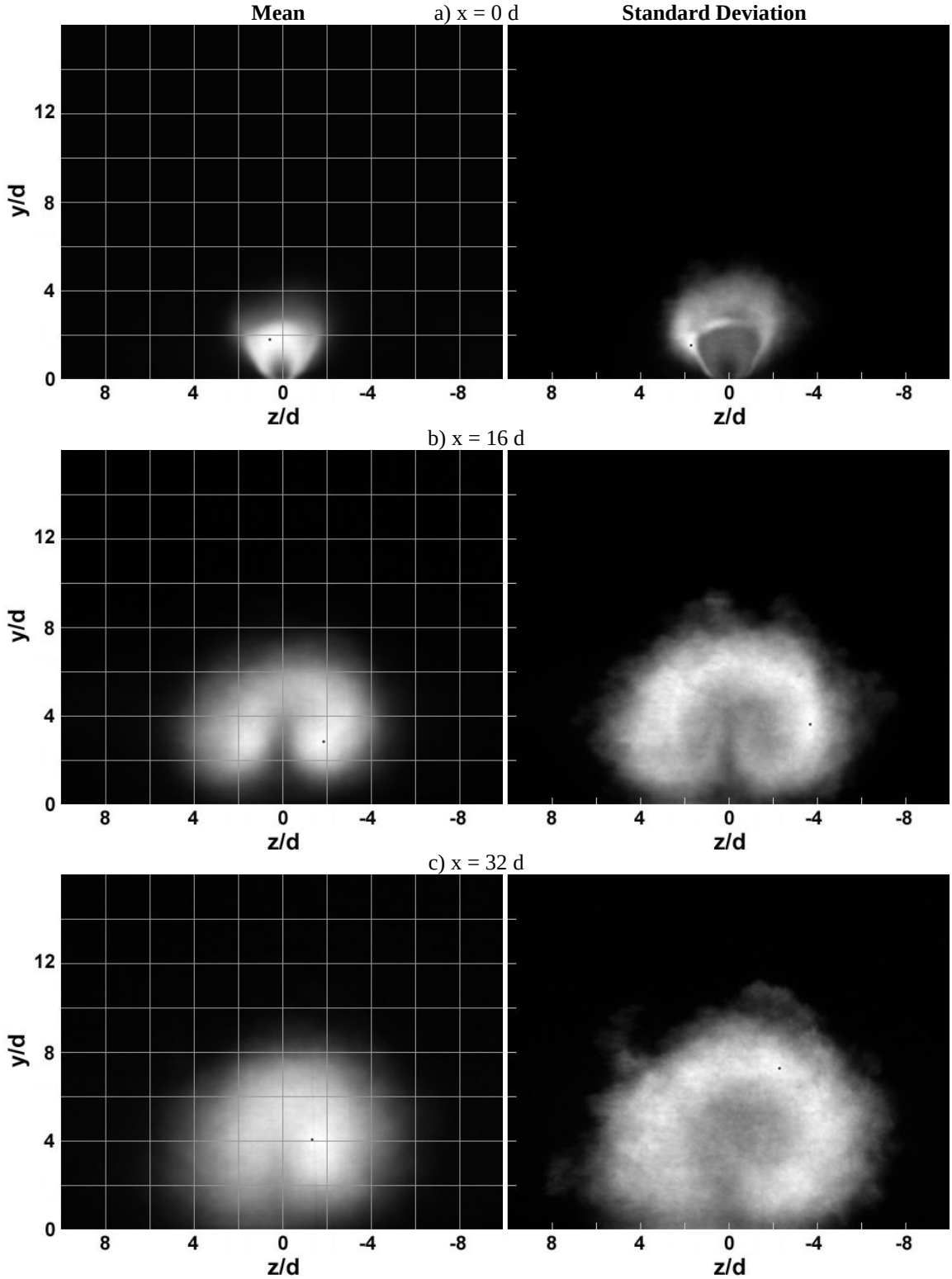

Figure 6. (F1) NO-PLIF, Flat insert, injection pressure 1, x/d = 0, 16, 32

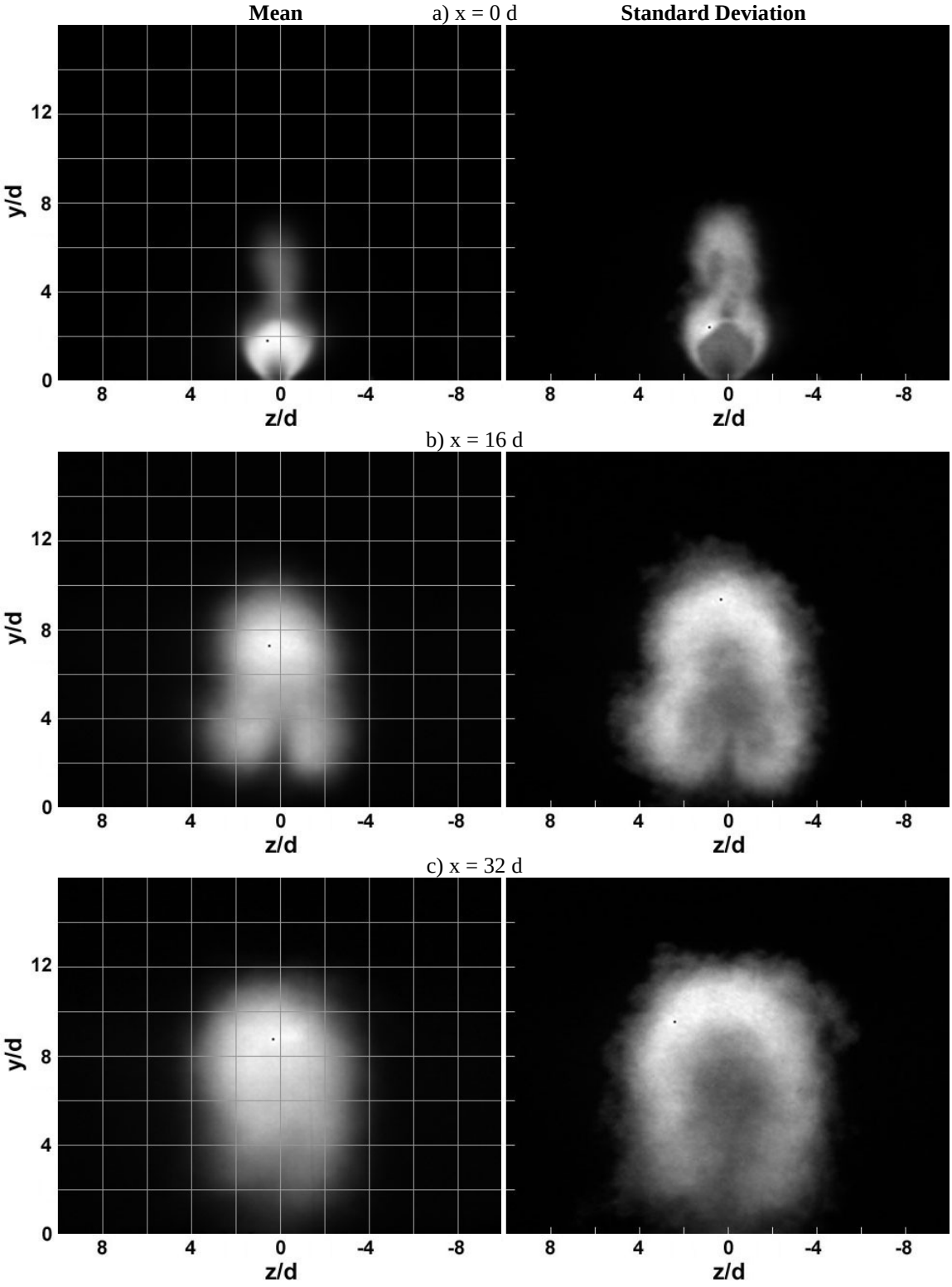

Figure 7. (M1) NO-PLIF, Medium pylon, injection pressure 1, x/d = 0, 16, 32

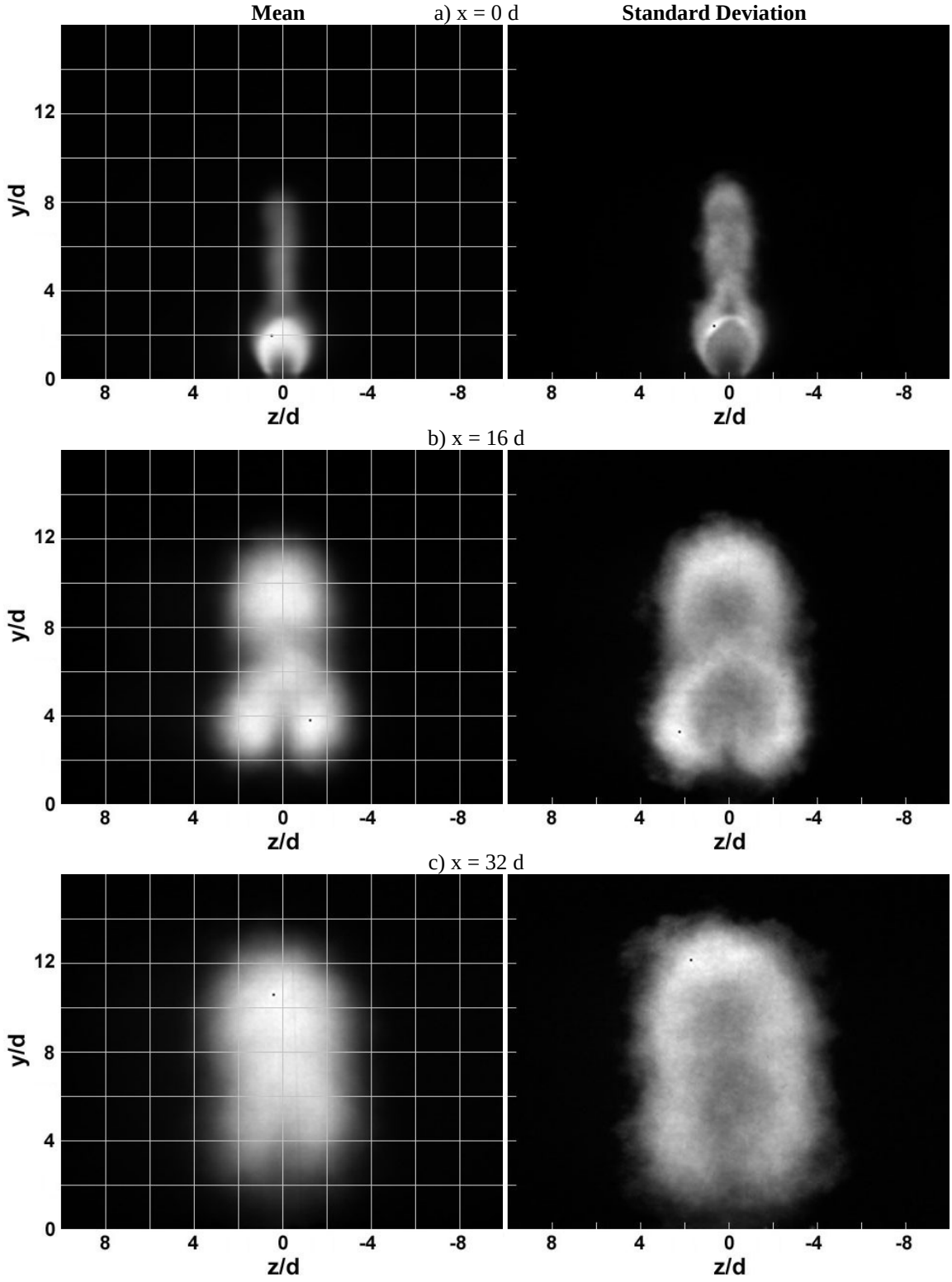

Figure 8. (T1) NO-PLIF, Tall pylon, injection pressure 1, x/d = 0, 16, 32

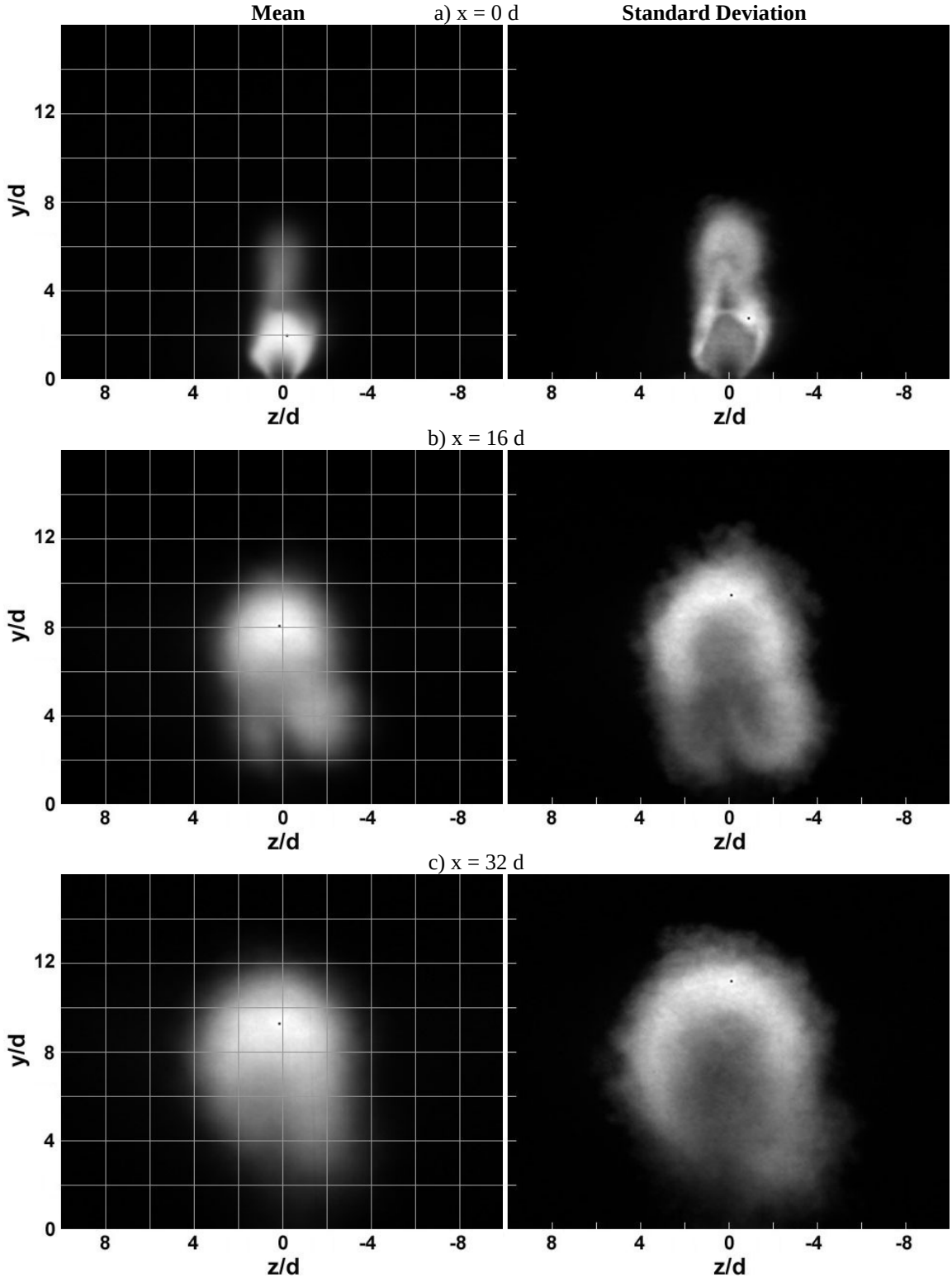

Figure 9. (W1) NO-PLIF, Wide pylon, injection pressure 1, x/d = 0, 16, 32

When no pylon is installed (Figure 6), the jet exhibits the familiar behavior observed in previous research.[8] At the jet injection location (x/d = 0), the jet crowns as it quickly expands, and it is mostly concentrated near the floor. The standard deviation at this location shows a large jet/core interaction over the top of the crown. The fluid then quickly develops into a lifted formation with counter-rotating edges. The mean images show that most of the jet is concentrated in these areas, while the standard deviation illustrates the strong interaction around the side and bottom of the plume. These areas of high interaction (bright white on the standard deviation images) are large and well defined at distances downstream. Even at high q, some of the jet fluid settles near the floor. This could result in fuel pooling in the boundary layer, a condition that can lead to flashback, especially in inlets.[2] Assessment of this condition cannot be completed in this mixing study, but measurements of the jet boundary and floor separation for each case provide an estimate.

When flow is injected behind the Medium pylon (Figure 7), the jet is observed to crown, but with a small amount of NO penetrating past the interaction layer and into the freestream (above the pylon). The jet then immediately widens to a thickness greater than the pylon, with a high interaction zone in the base area. By the x/d = 16 location, jet fluid has penetrated into the higher thin area seen before and is more concentrated. The familiar counter-rotating formations are evident but begin to play less of a role, as the standard deviation shows the interaction zone shifting up to match the lift in jet concentration. By x/d = 32, the majority of the jet fluid and interaction is in the upper area, which has become wider and more pronounced.

This three part process (immediate penetration and widening, transfer of fluid concentration away from the floor and counter-rotating areas, settling of the fluid in the now wide upper area) is observable in all three pylon configurations. The process suggests that the pylons generally lift fuel from the floor and disperse it higher into the cross-flow, lessening the vortex generation (less centrifugal effect) while maintaining a large interaction zone. All pylons also serve to increase the penetration height and leave the fuel higher off the floor over the Flat case. A lower q (not shown here) causes the developments to develop and become steady more quickly than with a higher q.

Injection behind the Tall pylon (Figure 8) shows immediate penetration past the crown such that the standard deviation shows a high initial level of development in the upper area. The crown does not have as defined of an interaction zone. The base then begins to widen, although not as rapidly as in the Medium case. At x/d = 16 there is roughly an equal level of jet concentration and interaction between the upper and lower areas. Here the shape distinctly shows there are almost two independent areas. The counter-rotating flow begins to fade farther downstream, and by x/d = 32 more fluid is concentrated in the upper area. This is the trend seen in the Medium case, but the Tall jet does not develop as quickly. The Tall case shows much higher penetration into the freestream. The upper and lower areas are more distinct and continue to develop on their own once formed. This shows that the Tall geometry provides ample room for fuel dispersion initially and downstream, mainly because of its large presence. It is still thin enough to allow vortex generating phenomena to affect the lower fuel area. The Tall pylon also noticeably lifts fuel off the boundary layer through the full range of injection pressures.

Injection behind the Wide pylon (Figure 9) exhibits many of the characteristics now established by the Medium and Tall cases. What sets the Wide configuration apart is the rapidness of jet penetration and initial upper area development. Upon injection the jet fluid, as well as the interaction zone, quickly penetrate to a height much higher than the pylon height, and by x/d = 8 (not shown) the transition from the lower to the upper area begins. As the jet lifts quickly off the floor, it slowly establishes its final form, settling somewhere around x/d = 24. This distance is larger than in the Medium case. All three injection pressures show the jet transitioning quickly and lifting from the floor, followed by a slow transition to the final form. This is advantageous, for the pylon quickly infuses fuel up into the core flow and then allows it to mix. In fact, local maximum standard deviation values (normalized by initial max intensity as discussed previously) show the most global interaction in the Wide case. A large floor gap is observed with the Wide pylon. Fuel does not remain in the boundary layer. Once again, this is related to preventing flashback.

Each pylon's maximum and minimum improvement over the Flat case for each injection pressure is presented in Table 2. These values are obtained from various streamwise locations and are based on geometric measurements discussed previously. The jet border is defined as 10% or greater intensity so that penetration height, jet width, and area can be measured (more explanation below).

Table 2. Basic jet geometries or each pylon compared to the no pylon case

		M1	M2	M3	T1	T2	T3	W1	W2	W3
$y_j / y_{j\,FLAT}$	max	1.67	2.03	2.38	2.06	2.54	2.88	1.71	2.06	2.35
	min	1.31	1.42	1.44	1.49	1.62	1.67	1.36	1.43	1.49
$\Delta z / \Delta z_{FLAT}$	max	0.88	0.79	0.82	0.72	0.70	0.82	0.76	0.81	0.88
	min	0.69	0.61	0.66	0.66	0.55	0.62	0.70	0.63	0.72
$A_j / A_{j\,FLAT}$	max	1.13	1.30	1.53	1.12	1.26	1.42	1.18	1.40	1.59
	min	0.90	0.90	0.94	0.93	0.94	1.02	0.82	0.91	0.99

Although Mie scattering provides an outline of the jet, it is not nearly as detailed and concentration-correlated as NO readings. Using the mean NO images, measurements were made on the maximum penetration height (y_j) and maximum vertical and horizontal spreads (Δy and Δz, respectively). The separation distance of the jet fluid from the test section floor is termed the floor gap (g) and was calculated as $g = y_j - \Delta y$. Jet area (A_j) was measured as the area in the mean images encompassed by at least 10% max intensity, in a manner similar to previous experiments.[9] Mixing area (A_s) was gathered from the standard deviation images as the area encompassed by an intensity value of 70% or greater. These two areas were measured by analyzing the histograms of each image and counting the appropriate number of pixels at a given brightness level percentage.

When q = 3, the Tall pylon creates a 105% increase in penetration height and as much as a 34% reduction in jet width. For q = 1.5, the same pylon causes a maximum y_j increase of 155% and a 45% reduction in width. At q = 0.75, the Tall pylon causes up to a 190% height improvement and a 38% width reduction. From the standpoint of fuel jet intensifying, the Tall pylon is the most effective. Injection pressure 3 exhibits the largest jet height improvement for all pylons. Injection pressure 2 causes the largest width reductions. The Wide and Medium pylons display many similar trends in their maximum abilities. This can be attributed to their physical size being very similar. The Wide pylon is better at providing penetration, whereas it has a slightly lower ability to shrink the lateral spread. Both generally show larger maximum jet areas than the Tall pylon, although the streamwise plots will show the Tall pylon as generally providing a larger area. These maximum and minimum data do not paint the full picture. Further details are discussed with the data plots shown next.

Error in measuring the borders of the images could range up to 10 image pixels when measuring visually.[10] This equates to about 1.7 jet diameters using the NO-PLIF conversion factor discussed in the data reduction section. Using the histogram method of capturing only the brightness values above 10% (or 70% in the standard deviation case), the error reduces to 1 – 2 pixels (0.4 d). The plots are presented without error bars to reduce clutter, noting that all the lines share the same error probability.

Figures 10 through 15 show the plot summaries of the various data measured. The values are based on the local maxima and minima of each end view image.

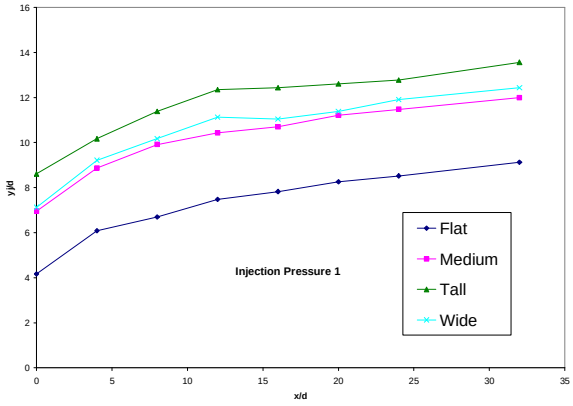

(a)

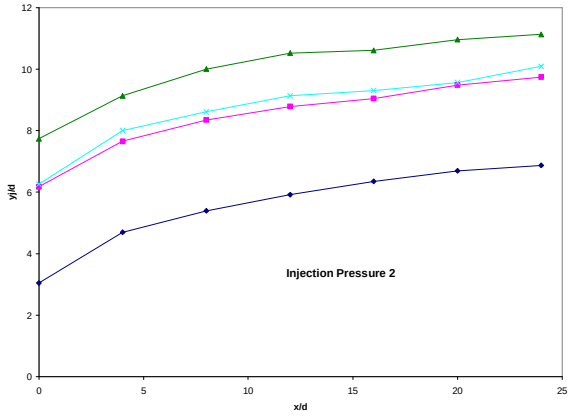

(b)

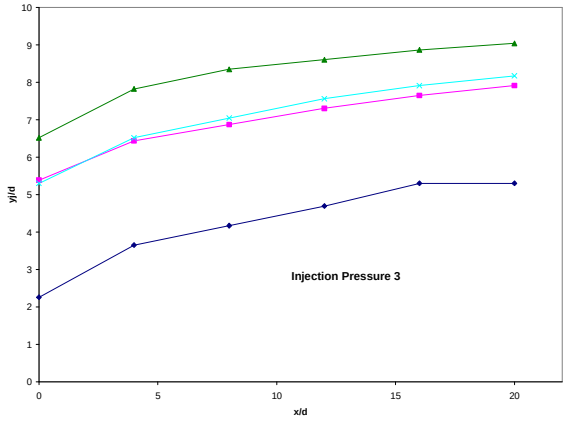

(c)

Figure 10. Penetration height (y_j/d) for injection 1 – 3

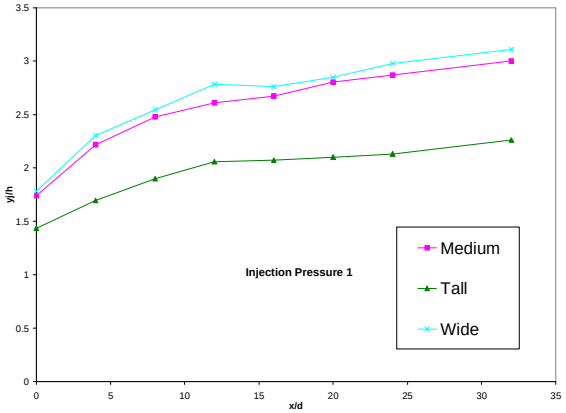

(a)

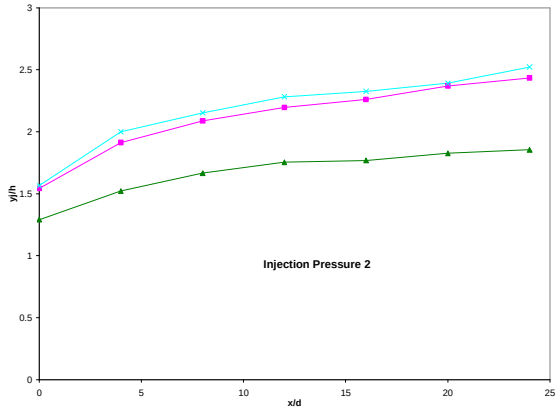

(b)

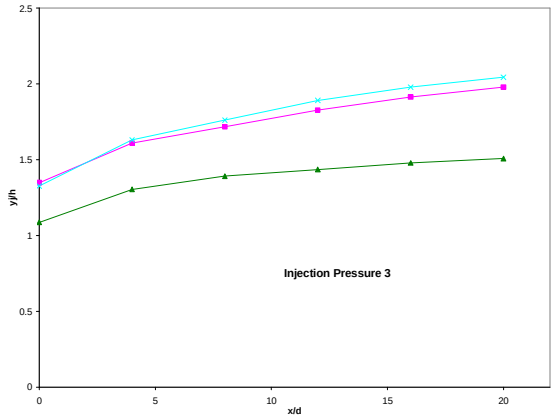

(c)

Figure 11. Penetration height with respect to pylon (y_j/h) for injection 1 – 3

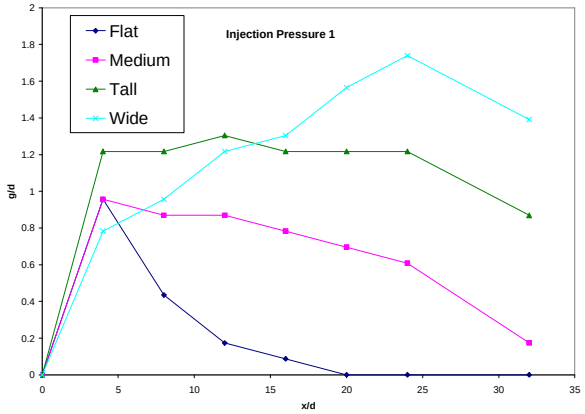

(a)

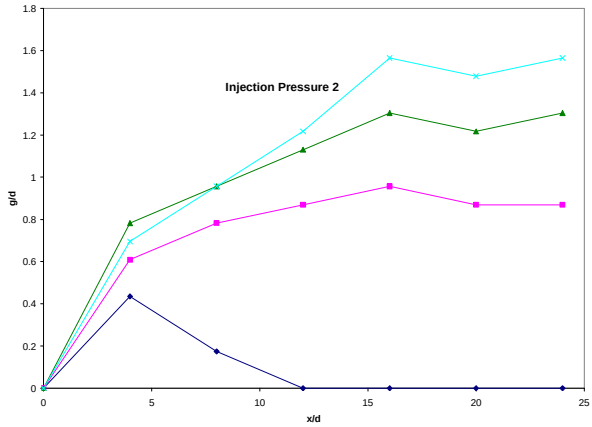

(b)

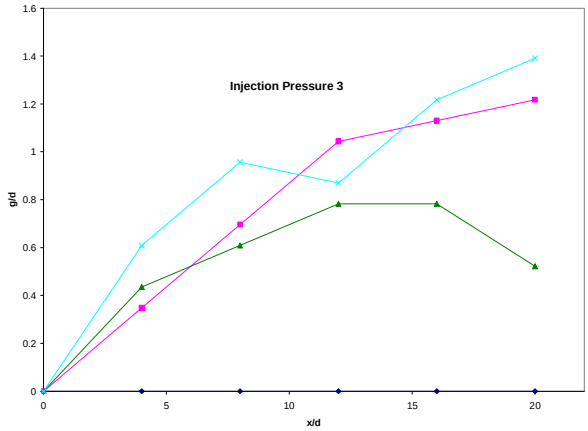

(d)

Figure 12. Floor gap (g) for injection 1 – 3

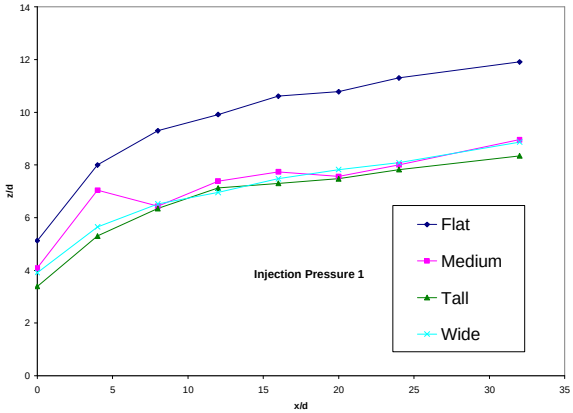

(a)

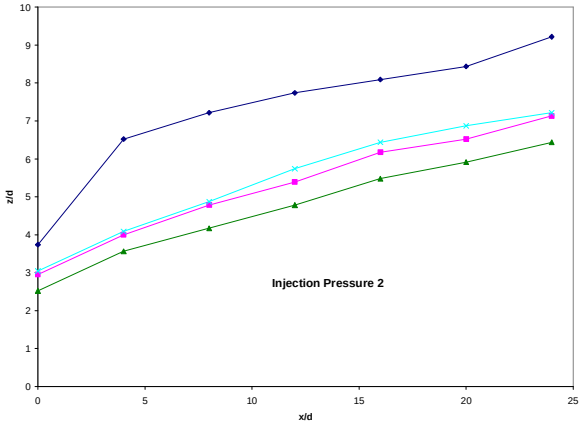

(b)

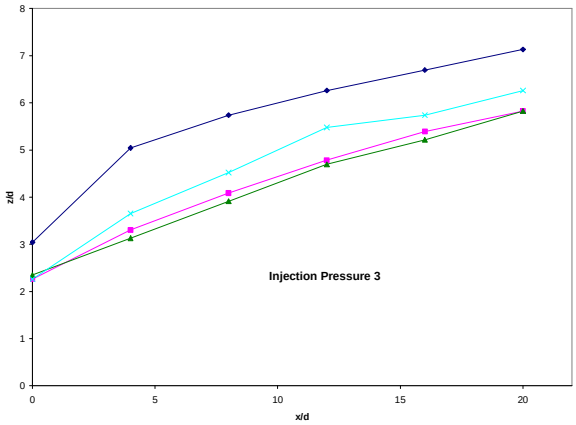

(c)

Figure 13. Width (Δz/d) for injection 1 – 3

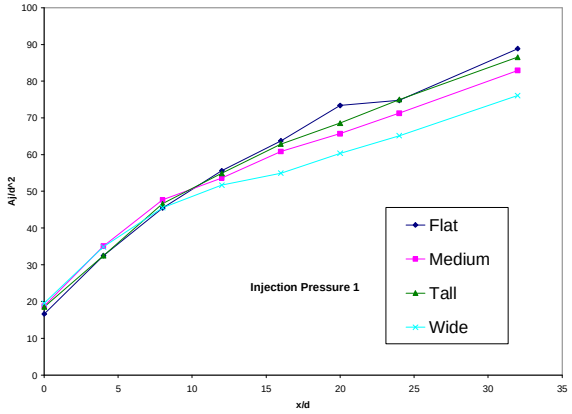

(a)

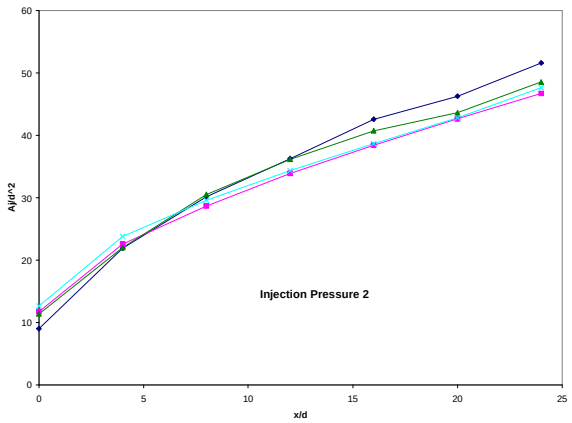

(b)

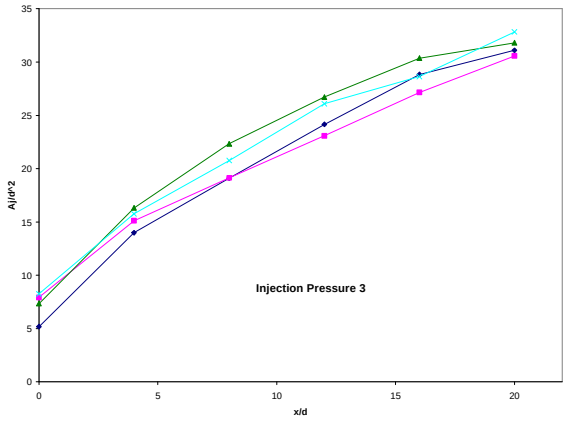

(e)

Figure 14. Jet area (Aj/d^2) for injection 1 – 3

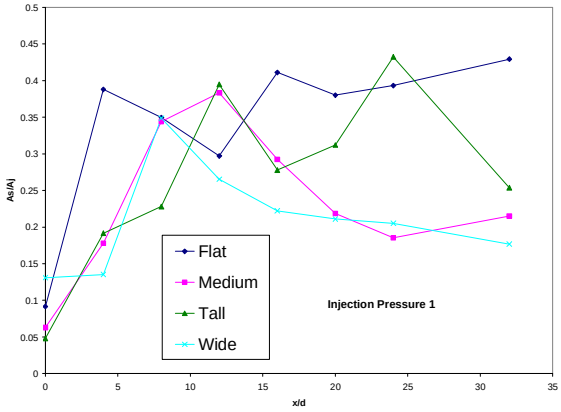

(a)

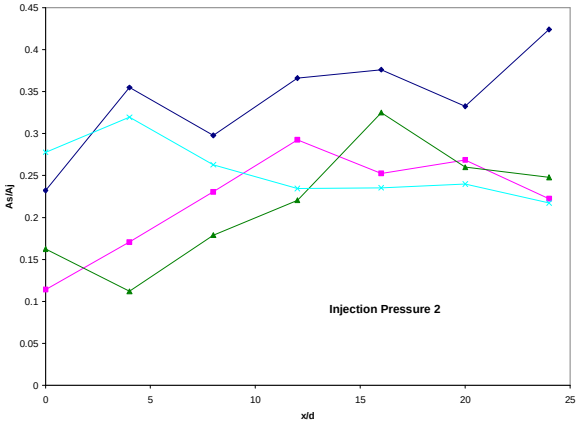

(b)

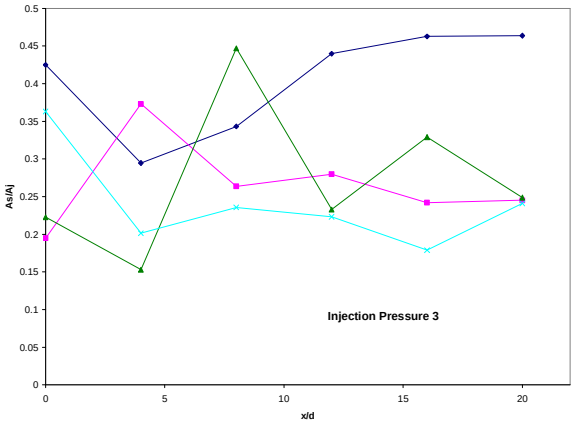

(c)

Figure 15. Local standard deviation area fraction (A_s/A_j) for injection 1 – 3

The Tall pylon shows an overwhelming advantage in pushing the fuel jet into the freestream (Figure 10). The Wide pylon has a slight advantage over the Medium, which actually contradicts the computational predictions by Gouskov et al which would have the Medium pylon providing a slightly higher penetration height.[4] All pylons push the jet fluid out higher than Flat injection. Introducing fluid high into the core flow will produce a larger fuel/air mixture over the cavity and may lift the cavity shear layer such as to transfer flameholder energy into the main stream.

The Wide pylon, which is the same height as the Medium pylon, shows a higher self normalized penetration height than its partner (Figure 11). Although the Tall provides more penetration height due solely to its size, design for minimum losses may dictate that a smaller pylon be used that exhibits a better y_j/h. This is more fuel efficient and incurs smaller shock losses. At x/d = 16, the Wide and Medium pylons exhibit a self normalized penetration height of greater than 1.5 (the average value observed in previous studies).[1-2, 4] This plot again shows the slight advantage the wide pylon has compared to the Medium pylon, which makes it a better choice given they produce similar losses.

Although visually the Flat case appears to lift much of the fuel completely away from the boundary layer, calculations based on the 10% max intensity consideration show that the effective floor gap is completely zero for the F3 case (Figure 12). The jet lifts initially with the higher two injection pressures but then loses its gap farther downstream; this does not guarantee flashback prevention. The Wide pylon is the most effective lifter. The Tall pylon loses its effectiveness as injection pressure is decreased, while the Medium loses effectiveness at higher q values. All the pylons provide good lifting mechanisms due to cross-stream shear.

Combined with plume height, width affects the area in which mixing potential may exist. The Wide pylon produces only a slightly greater plume width, and only at lower q values (Figure 13). The pylons all distribute the fuel vertically and do not allow it to remain spread out. The Wide pylon shows its influence in the visual images, where its width prevents the free stream from causing the larger vortices seen in the thinner pylons. The Tall pylon provides the thinnest spread, which corresponds to the jet being stretched more so along the vertical (y) axis. The Flat case, although it is not able to achieve the same penetration height as the pylons, visually shows a jet that is concentrated on the lower outer boundaries, giving it a larger horizontal spread.

The measurement of jet area is one composite means to qualitatively predict mixing potential.[10] Intensity results show that the jet is fairly equally diluted into the freestream for all four geometries. At the two higher injection pressures, the Flat case has a larger area than the pylons (Figure 14). The Tall pylon provides the best area of the three pylons, and it overcomes the Flat injection at the lower q, as does the Wide pylon. Because the pylons have less local area but more global interaction (as in the previous intensity discussion), it can be supposed that fuel is also mixed into the freestream beyond the scope of the image.

Local standard deviation is presented in Figure 15 as the area of high standard deviation (defined as 70% or greater max intensity) divided by the jet area. Flat injection shows a slightly greater local interaction (and area). At the lowest and highest injection pressures, the Tall pylon is close to the local capability of the Flat case. At x/d > 16, the Tall pylon outperforms the other two other pylons. None of the pylons exhibit as strong a vortex generation as the Flat case in the images. This results in lower standard deviation in the above graphs. More fuel is exchanged with the freestream.

The Mie scattering end view images show the development of two (sometimes three) shock formations as the image marches downstream. Table 3 displays the heights of the first two shocks for each case, based solely on visual estimation from the end view images. The upper (I) shock emanates along the pylon edge, as profile images will demonstrate. In the Flat case, this shock corresponds to the coincident bow shock that injection into the direct freestream creates. A secondary shock (II) begins to form around the jet boundary and becomes observable around x/d = 8 – 12. Shock widths were not measured due to a camera range that was too small to observe their full spanwise extent. The small range also resulted in some of the heights being unreadable in the larger shock (I) for injection pressures 1 and 2.

Figure 16 shows sample mean Mie scattering end view images.

Table 3. Shock heights measured from Mie end view images

x/d	F1		M1		T1		W1		F2		M2	
	I	II	I	II	I	II	I	II	I	II	I	II
0	6.5		9		10.5		9.5		5		8	
4	11		12.5		14		13.5		9		12	
8	14.5		16		17.5		16.5		12.5	5	15	7
12	18.5	7.5	19	9	20.5	9.5	20	9	16	7.5	18	9
16	21.5	9.5	22.5	11	23.5	13	23	12	19.5	10	21	11
20		11.5	25	14.5		14		14	23	12	24	13.5
24		14.5		16.5		16.5		16	25	14		15
32		19		20.5		21		20				

x/d	T2		W2		F3		M3		T3		W3	
	I	II	I	II	I	II	I	II	I	II	I	II
0	10		8		4		7		9.5		6	
4	13		12		8		10.5		12.5		10	
8	16		15.5	7	11.5	5	14	6.5	16		13	7
12	19	9	18.5	9	14.5	7	17	8.5	18.5	9	16	8.5
16	22	11	21.5	11	18	9.5	20	10.5	22	11	20	10.5
20	24.5	13	24	13.5	21	12	23.5	13			23	13
24		15.5		15.5								

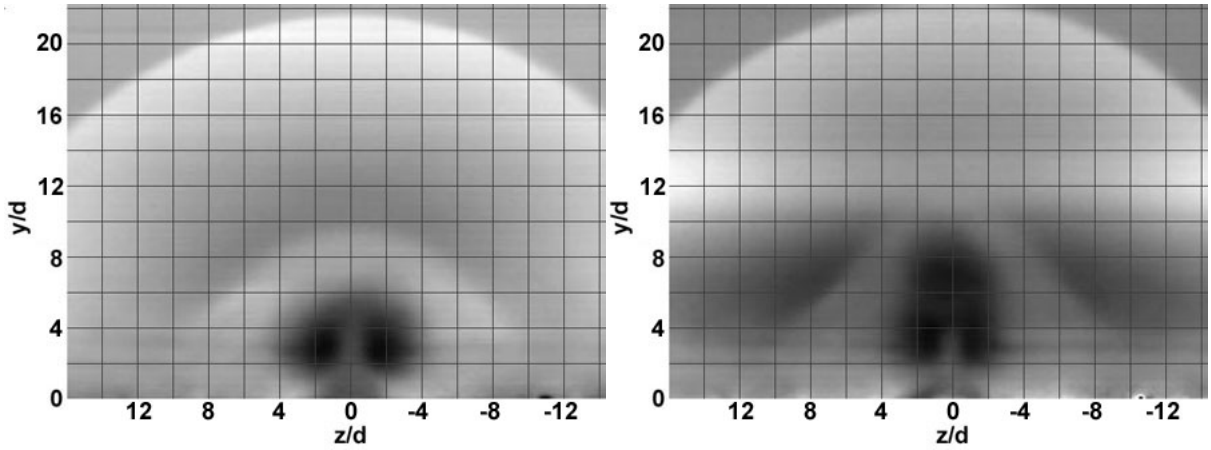

a) Flat b) Medium Pylon

Figure 16. Mean Mie scattering end view images at x/d = 16

The Medium and Wide pylons create shocks that are slightly stronger than the Flat case. The lower the injection pressure (3 being the lowest), the farther away from Flat values they become. For injection pressures 1 and 2, the Wide pylon creates somewhat stronger shocks (than the Medium), and at injection pressure 3 the Medium creates the stronger shocks. The Tall pylon generates the largest shock heights for all injection pressures. Based on only this data, the Tall pylon may not be a desirable geometry due to the overwhelmingly larger shocks it creates compared to the no pylon instance.

C. Profile Views

The following NO-PLIF images (Figures 21 through 26) are taken from the profile configuration, and each shows the general development of the jet in one picture. The profile views provide a visual representation of intensity reduction as well as a side-by-side comparison for penetration height between the Medium and the Flat injection. The Flat image correlates with other studies that observe similar jets under the same imaging methods.[9] A barrel shock and mach disc are visible. The pylon injection closely resembles the trend observed in liquid jet pylon studies.[1] The fluid is lifted beyond the height of the pylon and eventually settles at a certain height. This higher presence of fuel may interact with the shear layer over the cavity, but current data cannot support any hypotheses concerning actual shear layer behavior. For all three injection pressures, the pylon case outperforms the no pylon case by a noticeable margin.

The largest improvement in penetration height in these examples is in the M3 case (Figure 26). Visually there is a clear improvement of over 100%. Table 2 confirms this with a maximum value of 138% increase.

Shocks are barely visible in these profile images. This occurs because the UG-5 filter employed for NO-PLIF does not completely block out all the scattering at 226 nm. The shocks that are clearly visible in the Mie images therefore make themselves slightly apparent in the PLIF pictures.

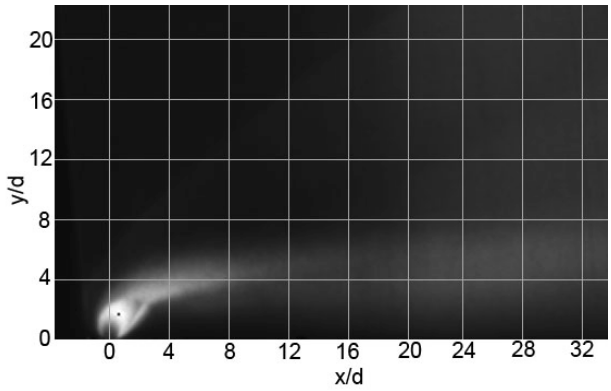

Figure 21. F1 case, NO-PLIF profile view

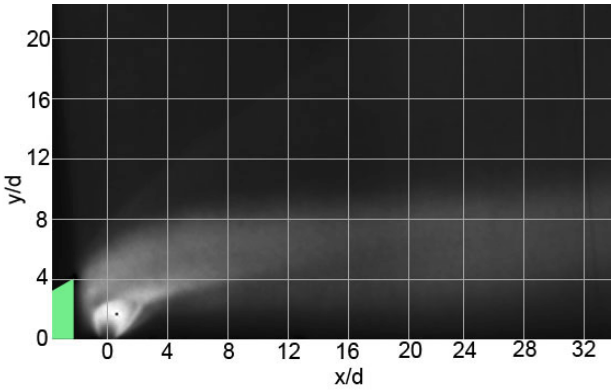

Figure 22. M1 case, NO-PLIF profile view

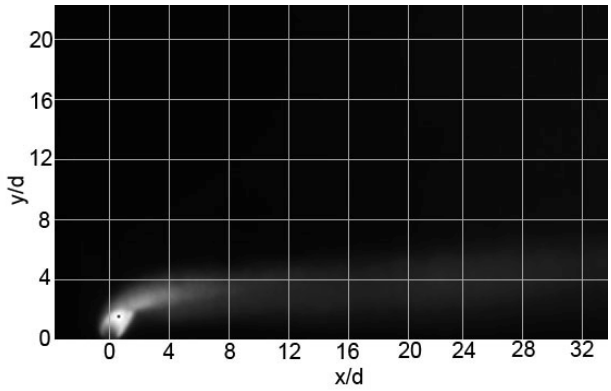

Figure 23. F2 case, NO-PLIF profile view

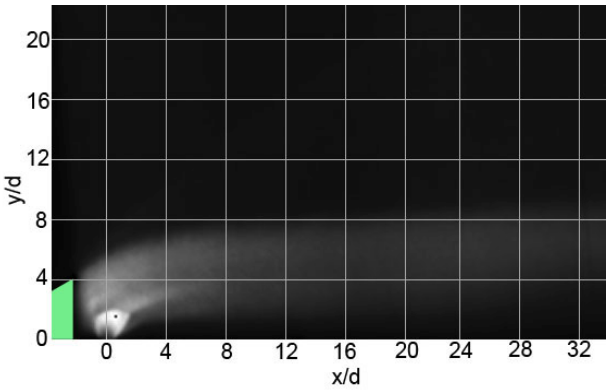

Figure 24. M2 case, NO-PLIF profile view

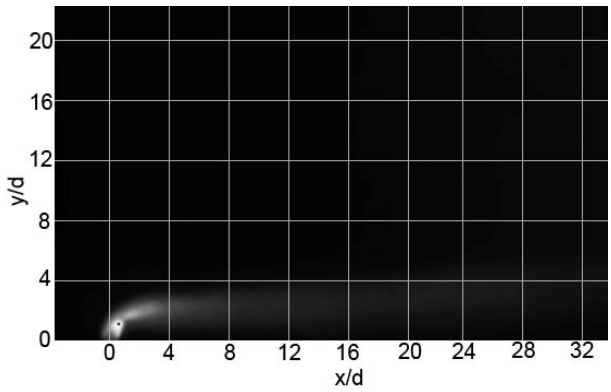

Figure 25. F3 case, NO-PLIF profile view

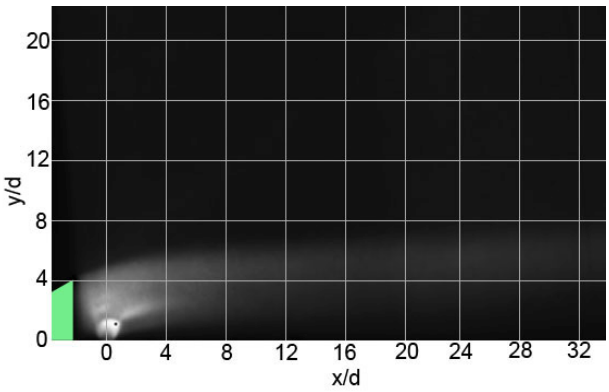

Figure 26. M3 case, NO-PLIF profile view

IV. Discussion and Conclusions

Three pylons were installed in turn upstream of a transverse circular injector in order to qualify any improvements that they made on fueling. Tests were conducted in a Mach 2 flow environment within a test section simulated to act like a supersonic combustor. The injection took place upstream of a cavity flameholder similar in design to cavities employed in functional scramjets. Data were acquired visually using Mie scattering and NO-PLIF measurements. Twelve configurations were tested in "scramjet" mode with completely supersonic flow. An additional reading (Medium pylon but no injection) was also conducted.

Mean intensity plots showed that the jet mixes into the freestream fairly consistently with a 95% dilution by the last streamwise readings. Standard deviation intensities demonstrated that more interaction was taking place in the farfield with pylons than without (it was highest in the Wide case). With a high enough injection pressure, pylons created a high intensity of standard deviation directly downstream of injection.

Raw images from both the Mie scattering and the NO-PLIF runs display large, turbulent structures that demonstrate a considerable opportunity for mixing interaction. This information is not intuitive from the averaged images.

Flat injection showed solid development of counter-rotating vortices, a wide profile, the largest jet area, and the most local standard deviation. Medium pylon injection creates an initially wide jet, and the vortices are not as much an influence. Fluid eventually moves to the top formation. The higher the injection pressure the longer it takes to develop. The Medium pylon causes the most jet width normalized by pylon width. At the higher injection pressures it has the lowest floor clearance of the three pylons. The Tall pylon immediately penetrates past the crown, but development of the remainder of the average structure is slower than the other pylons. This pylon is a very effective fuel penetrator that causes the highest vertical penetration and width reduction of all the inserts. It provides a considerable floor clearance (only behind the Wide pylon) and contains the same or better jet area as the Flat case. The Tall also creates a significant amount of local standard deviation. The Wide pylon demonstrates immediate penetration followed by a very slow development relative to the other pylons. Its causes very high fuel heights when normalized by pylon height, and the second largest total fuel height. Injection behind this pylon quickly lifts from the floor, suggesting a significant baroclinic torque or cross-stream shear effect. The floor gap is the highest of the pylons in the farfield. This pylon also exhibits medium to low standard deviation compared to the other inserts, suggesting that its vortices are not as much as an influence.

The Medium and Wide pylons create similar bow shock magnitudes that are slightly higher than the Flat injection. The Tall pylon causes much larger shocks. High q injection behind the Medium pylon produced almost as low shock heights as the same q injection with no pylon. Low q injection behind the Medium pylon did not affect the shock heights present when there was no injection. The pylon effectively shielded the entire jet, allowing it to achieve high penetration.

This research produced the following conclusions:

1) All the pylons provided more penetration and less lateral spread than the Flat injection. All the pylons lifted the fuel off the floor at all values of q, suggesting that flashback is preventable using this injection method. The pylons showed less local standard deviation activity (seen in the images), but intensity plots show that all the pylons were interacting with and diluting into the freestream at the same level or more than in the Flat case.

2) The Tall pylon was designed to be of a larger scale than the other two pylons. It was based on the optimal geometry obtained from a computational study. The greater size of this pylon (more than its shape) is what effected the large penetration height. Unfortunately, h/d = 6 created stronger shocks than the other three cases. Based on shock heights alone, the Tall incurred between a 10 – 50% additional drag penalty compared to the smaller pylons. Pylon height should be kept to a value of 4 d or below to minimize losses.

3) The Wide pylon was the best performer overall. It lifted the fuel jet away from the boundary layer quickly and established a good penetration height. This pylon was designed with the second best geometry suggested by computational research but performed better than the Medium pylon of the same height (designed with the optimal suggested geometry). Further profile view analysis would probably yield a similar shock trend as exhibited by the Medium pylon, as suggested by end view shock measurements.

4) The lowest dynamic pressure ratio resulted in fuel being completely shielded behind the pylons and having no additional effect on shock losses. This injection pressure achieved the most drastic pylon aided fuel height increase over Flat injection. The Wide pylon at q = 0.75 enhanced penetration height by 135% (105% for q = 1.5, 70% for q = 3).

5) The qualitative approach to determining mixing potential warrants more detailed experimentation. The presence of pylons reduced the formation of counter-rotating vortices while increasing the profile of the fuel jet. Although the standard deviation with pylons installed was greater on a global scale, more information is required to form a link between pylons and mixing potential.

.

Acknowledgments

The first and second authors would like to acknowledge the support of AFRL/PR. The authors would also like to acknowledge the support Bill Terry and Dave Schommer of ISSI in wind tunnel operations.

The views expressed in this article are those of the author and do not reflect the official policy or position of the United States Air Force, Department of Defense, or the U.S. Government.

References

[1]Livingston, T., and Segal, C., "Penetration and Spreading of Liquid Jets in an External-Internal Compression Inlet," *AIAA Journal*, Vol. 38, No.6, 2000, pp. 989-994.

[2]Owens, M.G., Mullagiri, S., and Segal, C., "Effects of Fuel Preinjection on Mixing in Mach 1.6 Airflow," *Journal of Propulsion and Power*, Vol. 17, No. 3, 2001, pp. 605-610.

[3]Gruber, M.R., Donbar, J.M., Carter, C.D., and Hsu, K.-Y., "Mixing and Combustion Studies Using Cavity-Based Flameholders in a Supersonic Flow," *Journal of Propulsion and Power*, Vol. 20, No. 5, 2004, pp. 769-778.

[4]Gouskov, O., Kopchenov, V., and Vinogradov, V., "Numerical Researches of Gaseous Fuel Pre-Injection in Hypersonic 3-D Inlet," AIAA Paper 2000-3599, July 2000.

[5]Gruber, M.R., and Nejad, A.S., "New Supersonic Combustion Research Facility," *Journal of Propulsion and Power*, Vol. 11, No. 5, 1995, pp. 1080-1083.

[6]Lee, M.P., McMillin, B.K., Palmer, J.L., and Hanson, R.K., "Planar Fluorescence Imaging of a Transverse Jet in a Supersonic Cross Flow," *Journal of Propulsion and Power*, Vol. 8, No. 4, 1992, pp. 729-735.

[7]VanLerberghe, W.M., Santiago, J.G., Dutton, J.C., and Lucht, R.P., "Mixing of a Sonic Transverse Jet Injected into a Supersonic Flow," *AIAA Journal*, Vol. 38, No.3, 2000, pp. 470-479.

[8]Cortelezzi, L., and Karagozian, A.R., "On the Formation of the Counter-rotating Vortex Pair in Transverse Jets," *Journal of Fluids*, Vol. 446, 2001, pp. 347-373.

[9]Murugappan, S., and Gutmark, E., "Control of a Transverse Supersonic Jet Injection into a Supersonic Cross-Stream," AIAA Paper 2004-1204, January 2004.

[10]Gruber, M.R., Nejad, A.S., Chen, T.H., and Dutton, J.C., "Transverse Injection from Circular and Elliptic Nozzles into a Supersonic Cross Flow," *Journal of Propulsion and Power*, Vol. 16, No. 3, 2000, pp. 449-457.